JACS
JOURNAL OF THE AMERICAN CHEMICAL SOCIETY

ARTICLE

pubs.acs.org/JACS

^{57}Fe ENDOR Spectroscopy and 'Electron Inventory' Analysis of the Nitrogenase E_4 Intermediate Suggest the Metal-Ion Core of FeMo-Cofactor Cycles Through Only One Redox Couple

Peter E. Doan,[†] Joshua Telser,[†,¶] Brett M. Barney,[‡] Robert Y. Igarashi,[‡] Dennis R. Dean,[§] Lance C. Seefeldt,[‡] and Brian M. Hoffman*[,†]

[†]Department of Chemistry, Northwestern University, Evanston, Illinois 60208, United States

[‡]Department of Chemistry and Biochemistry, Utah State University, Logan, Utah 84322, United States

[§]Department of Biochemistry, Virginia Tech, Blacksburg, Virginia 24061, United States

Supporting Information

ABSTRACT: N_2 binds to the active-site metal cluster in the nitrogenase MoFe protein, the FeMo-cofactor ([7Fe-9S-Mo-homocitrate-X]; FeMo-co) only after the MoFe protein has accumulated three or four electrons/protons (E_3 or E_4 states), with the E_4 state being optimally activated. Here we study the FeMo-co ^{57}Fe atoms of E_4 trapped with the α-70$^{Val\rightarrow Ile}$ MoFe protein variant through use of advanced ENDOR methods: 'random-hop' Davies pulsed 35 GHz ENDOR; difference triple resonance; the recently developed Pulse-Endor-SaTuration and REcovery (PESTRE) protocol for determining hyperfine-coupling signs; and Raw-DATA (RD)-PESTRE, a PESTRE variant that gives a continuous sign readout over a selected radiofrequency range. These methods have allowed experimental determination of the signed isotropic ^{57}Fe hyperfine couplings for five of the seven iron sites of the reductively activated E_4 FeMo-co, and given the magnitude of the coupling for a sixth. When supplemented by the use of sum-rules developed to describe electron-spin coupling in FeS proteins, these ^{57}Fe measurements yield both the magnitude *and* signs of the isotropic couplings for the complete set of seven Fe sites of FeMo-co in E_4. In light of the previous findings that FeMo-co of E_4 binds two hydrides in the form of (Fe-(μ-H$^-$)-Fe) fragments, and that molybdenum has not become reduced, an 'electron inventory' analysis assigns the formal redox level of FeMo-co metal ions in E_4 to that of the resting state (M^N), with the four accumulated electrons residing on the two Fe-bound hydrides. Comparisons with earlier ^{57}Fe ENDOR studies and electron inventory analyses of the bio-organometallic intermediate formed during the reduction of alkynes and the CO-inhibited forms of nitrogenase (hi-CO and lo-CO) inspire the conjecture that throughout the eight-electron reduction of N_2 plus 2H$^+$ to two NH_3 plus H_2, the inorganic core of FeMo-co cycles through only a single redox couple connecting two formal redox levels: those associated with the resting state, M^N, and with the one-electron reduced state, M^R. We further note that this conjecture might apply to other complex FeS enzymes.

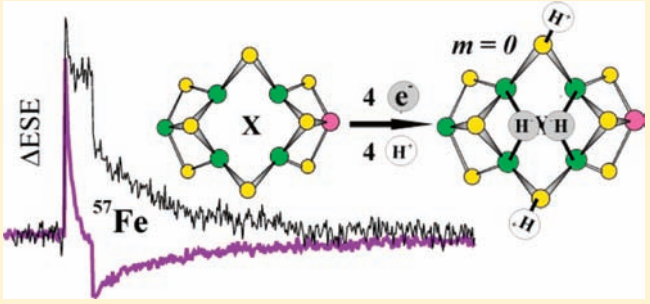

INTRODUCTION

Nitrogenase catalyzes the biological reduction of dinitrogen (N_2) by protons and electrons in a reaction in which one mole of dihydrogen is produced along with two moles of ammonia according to the ideal stoichiometry of eq 1:[1−4]

$$N_2 + 8e^- + 16MgATP + 8H^+ \rightarrow 2NH_3 + H_2 + 16MgADP + 16P_i \quad (1)$$

Mo-dependent nitrogenase is composed of two component proteins; the Fe protein and the MoFe protein. The Fe protein delivers electrons to the MoFe protein in a reaction requiring the hydrolysis of a minimum of 2 MgATP per electron transferred. The MoFe protein contains two unique metal cluster types; the P cluster (8Fe-7S), and the iron/molybdenum cofactor of nitrogenase (FeMo-cofactor; [FeMo-co]) [7Fe-9S-Mo-homocitrate-X]),[5−8] where substrates bind and react, Figure 1.[8−11] A series of studies that combined genetic, biochemical, and spectroscopic approaches have: (i) identified the site of reactivity on FeMo-co as the face defined by Fe atoms 2, 3, 6, and 7 (numbering based on PDB structure 1M1N); (ii) demonstrated that the side chain of residue α-70^{Val} acts as a 'gatekeeper' that controls access to the FeMo-co active site; and (iii) supported the idea that proton delivery involves the side chain of residue α-195^{H}.[4,12,13]

N_2 reduction by nitrogenase proceeds along a reaction pathway comprising a sequence of intermediate states generated as

Received: June 8, 2011
Published: October 07, 2011

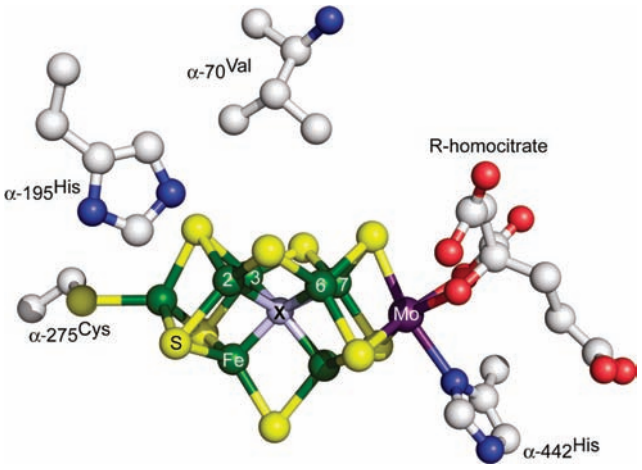

Figure 1. Structure of the FeMo-cofactor showing Fe green, Mo purple, S yellow, **X**, gray.

eight e^-/H^+ are delivered to the MoFe protein and a dinitrogen bound to FeMo-co undergoes six steps of hydrogenation,[1,3,4,14−16] with the $[Fe_4S_4]$ cluster of the partner Fe protein delivering electrons to the MoFe protein one at a time in a reaction requiring the hydrolysis of a minimum of two MgATP molecules per electron transferred.[1] The stepwise reductive activation of the MoFe protein, followed by the stepwise reduction of N_2 is schematized in the Lowe−Thorneley (LT) kinetic model for nitrogenase function[1,17,18] which is formulated in terms of states, denoted E_n, that are indexed by the number of electrons and protons, n, that have been delivered to the MoFe protein during their formation: $n = 0$ (resting) ↔ 8 (as required by eq 1). N_2 does not bind until the MoFe protein has accumulated either three or four electrons and protons, E_3 or E_4, with optimal reductive activation at E_4,[17] and N_2 binding is accompanied by the obligatory liberation of H_2. In the absence of other substrates, activation of MoFe protein leads to the reduction of protons to form H_2, with the protein thereby cycling back to its resting state.

An understanding of the nitrogenase mechanism must incorporate an understanding of the electronic structure of FeMo-co for each E_n stage. Mössbauer spectroscopy,[19] assisted by electron nuclear double resonance (ENDOR) spectroscopy,[20] has characterized the seven Fe ions of FeMo-co in the resting state of the MoFe protein (E_0), and ENDOR spectroscopy has characterized the Mo.[21] This information has been integrated by broken-symmetry DFT computation into a consensus assignment of the metal-ion valencies of the resting FeMo-co (denoted as M^N) as, [3Fe(III), 4Fe(II), Mo(IV)], based on the presumption that X = N(−III), and of the scheme by which the high-spin Fe(III) and Fe(II) ions spin-couple to achieve the $S = 3/2$ total spin state of M^N.[22−24]

The next stage in understanding the electronic structure of FeMo-co during catalysis includes the study of the metal ion in reduced states (E_{1-4}) that are accessed during the activation required for N_2 binding, and of subsequent states along the N_2 reaction pathway, those in which FeMo-co has bound N_2 and its reduction intermediates. Beginning in 2004, a series of reports described the first freeze−quench trapping and characterization of enzymatic intermediates:[25,26] initially ones that form during the reduction of alkyne substrates,[27,28] then one formed during the reduction of H^+ under Ar,[29] then intermediates associated with N_2 reduction.[30−33] The trapping of these intermediates has inspired ongoing efforts to characterize both the substrate-derived fragments bound to the FeMo-co in these intermediates, through $^{1,2}H$, $^{14,15}N$, and ^{13}C ENDOR spectroscopy, and the metal ions of FeMo-co itself through ^{57}Fe[28] and ^{95}Mo[34] ENDOR measurements.

However, even when an intermediate has been trapped, this occurs without synchronous electron delivery to the MoFe protein. As a result, the number of electrons and protons, n, delivered to MoFe during formation of the intermediate is unknown, and thus it is untethered from the LT kinetic scheme for substrate reduction. This makes it extraordinarily difficult to relate the properties of the FeMo-co metal ions of the different intermediates to each other and to those of M^N.

To date, n has been determined unambiguously for only one freeze-trapped intermediate. When α-$70^{Val\rightarrow Ile}$ substituted MoFe protein under Ar reduces protons in the presence of Fe protein, reductant, and ATP, the EPR signal of M^N disappears, and this is accompanied by the appearance of an $S = 1/2$ signal from a trapped intermediate state. In this MoFe variant the enlarged side chain of α-70^{Ile} physically precludes the ready access of all substrates except protons without altering the reactivity of FeMo-co.[4] The application of a step-annealing relaxation protocol to the intermediate surprisingly showed that it is the E_4 kinetic state, which is the state optimally activated for N_2 binding through the accumulation by the MoFe protein of $n = 4$ electrons and protons relative to resting MoFe protein.[35] ENDOR spectroscopy revealed that E_4 contains two hydrides bound to FeMo-co.[29] The form of their hyperfine tensors rules out their binding as terminal ligands to either Mo or Fe, and indicates instead that they bridge two metal ions[36,37] as [Fe-(μ-H^-)-Fe] and/or [Mo-(μ-H^-)-Fe] fragments.[4,38] A subsequent ^{95}Mo ENDOR study on the isotopically enriched E_4 intermediate indicated it retained molybdenum in the Mo(IV) state and gave evidence the Mo is not involved in hydride binding, further favoring the [Fe-(μ-H^-)-Fe] mode of binding.[34]

As E_4 is the optimal state for N_2 binding,[1,17,18] it is of paramount importance to characterize the properties of this reductively activated FeMo-co, which require an understanding of the bonding, spin coupling, and reactivity of this state. To complete the experimental foundation for this program we build on the previous characterization of the Mo ion and hydride ligands through a study of the iron ions. Although Mössbauer spectroscopy was extraordinarily successful in characterizing the ^{57}Fe ions of resting-state FeMo-co (M^N),[19,39] the study of intermediates with this technique is problematic.[40] We have therefore applied newly developed ENDOR methods[41,42] to characterize the Fe ions of FeMo-co in the E_4 state of the α-$70^{Val\rightarrow Ile}$ MoFe protein isotopically enriched in ^{57}Fe. These methods have allowed experimental determination of the signed isotropic ^{57}Fe hyperfine couplings for five of the seven iron sites of the reductively activated E_4 FeMo-co, and given the magnitude of the coupling for a sixth. When supplemented by the use of sum-rules developed to describe electron-spin coupling in Fe−S proteins,[43] these ^{57}Fe measurements yield the signed isotropic couplings for the complete set of seven Fe sites of FeMo-co in E_4.

Incorporation of the finding that FeMo-co of E_4 binds two hydrides[29] into an 'electron inventory' analysis[44] has further allowed us to assign the redox state of FeMo-co in E_4 relative to that of resting state FeMo-co (E_0). This assignment enables a discussion of the correlation of the hyperfine couplings with FeMo-co redox levels and a reassessment of the redox levels assigned in earlier ^{57}Fe ENDOR studies of the CO-inhibited forms of WT nitrogenase (hi-CO and lo-CO)[44,45] and of bio-organometallic, alkene-bound intermediates.[28,46] These considerations in turn lead us to propose that electron accumulation by the MoFe protein during catalysis

involves the continual shuttling of electrons to a substrate while the metal ions of the inorganic core of FeMo-co cycle through only one redox couple. We further discuss the proposal that the activation of FeMo-co for the binding and reduction of N_2 through formation of E_4 involves a structural rearrangement.

MATERIALS AND METHODS

Protein Purification and Activity Assays. An *Azotobacter vinelandii* (*Av*) strain (DJ1373) expressing the α-70^{Ile} variant MoFe protein was constructed using a site-directed mutagenesis and gene replacement protocol as previously described.[47] The WT and α-70^{Ile} variant MoFe proteins were purified using a poly-His metal affinity chromatography system described earlier.[47] For ^{57}Fe-incorporated MoFe proteins, cells were grown with equivalent molar amounts of ^{57}Fe (100 mg equivalents/100 L of culture media) that was substituted for $FeSO_4$ (500 mg/100 L of culture media) normally added to the fermenter growth media. ^{57}Fe metal (95%, Cambridge Isotope Laboratories) was oxidatively dissolved in minimal amount of concentrated nitric acid (37%) with additional HCl (0.5 M), and this ^{57}Fe solution was added to the culture media in lieu of $FeSO_4$. *Av* cultures with ^{57}Fe were grown with limiting ammonium and were harvested 4 h after the consumption of the ammonium. The WT Fe protein component of nitrogenase was purified essentially as previously described.[48] All manipulations of proteins were conducted in septum-sealed serum vials under an argon atmosphere and all anaerobic liquid and gas transfers were performed using gastight syringes. Acetylene reduction and H_2 evolution activities were determined as described earlier.[49,50]

Preparation of Turnover MoFe Protein Samples for ENDOR. Turnover samples of the α-70^{Ile} Mo^{57}Fe protein (150 μM) were prepared in 100 mM MOPS buffer (pH 7.0), containing 5 mM ATP, 7.5 mM $MgCl_2$, 30 mM phosphocreatine, 30 mM dithionite, 2 mg/mL BSA, and 0.3 mg/mL creatine phosphokinase, and 75 μM Fe protein. The samples were prepared in 35 GHz EPR/ENDOR tubes. The reaction was allowed to progress at room temperature (~23 °C) for ~20 s and was quenched by freezing in liquid N_2.

ENDOR Measurement and Analysis. CW 35 GHz EPR and ENDOR spectra were recorded on a modified Varian E-110 spectrometer equipped with a helium immersion dewar at 2 K under 'rapid passage' conditions using 100 kHz field modulation.[51] CW ENDOR employed random noise broadening of the radio frequency (rf), which improves signal intensity.[52] Pulsed 35 GHz ENDOR spectra were obtained at 2 K on a locally constructed spectrometer.[53] CW spectra were collected either by linearly sweeping the rf or with the stochastic ENDOR protocol in which the rf is randomly hopped over the frequency range of the spectrum, with background subtraction, [rf-on] − [rf-off], at each frequency.[54] The Davies pulse sequence[55] was implemented with random hopping of the rf over the frequency range for a spectrum, but without background subtraction.[56] Each procedure improves intensity and eliminates distortions of signal shapes caused by slow nuclear relaxation. In each procedure, the order of the entire set of frequencies is permuted prior to the acquisition of a single transient for each frequency. After the entire set of frequencies is exhausted, the set of frequencies is permuted again and procedure is repeated. Data acquisition for all pulse experiments utilized the SpecMan software package[57] (http://specman.4epr.com) in conjunction with a SpinCore PulseBlaster ESR_PRO 400 MHz word generator and an Agilent Technologies Acquiris DP235 500 MS/s digitizer. The ENDOR pattern for a single orientation of an $I = 1/2$ nucleus with relatively large hyperfine coupling and small g_N, as is the case for ^{57}Fe, exhibits a $\nu_{+/-}$ doublet that is centered at half the hyperfine coupling, $|A/2|$, and split by twice the nuclear Larmor frequency, $2\nu_N$,

$$\nu_{\pm} = |A/2 \pm \nu_N| \quad (2)$$

for ^{57}Fe, $\nu_{Fe} \approx 3.4$ MHz ($g \approx 2.0$, $\nu_{mw} \approx 35$ GHz, $B_0 = 1.25$ T).

Use of Difference Triple to Correlate ν_+/ν_-. The complexity of the ENDOR patterns from multiple ^{57}Fe sites requires use of a method specifically able to correlate the $\nu_{-/+}$ branches of a single ^{57}Fe center in order to complete the assignments to individual sites. One commonly used for this purpose is hyperfine-selective sublevel correlation or HYSCORE, a two-dimensional (2D) electron-spin−echo modulation-based technique which has been recently demonstrated on ^{57}Fe centers with hyperfine interactions of $|A| \approx 12$ MHz in Fe-hydrogenase.[58] However, the larger interactions ($|A| > 20$ MHz) observed in this work combined with the small values of $2\nu(^{57}Fe)$ relative to the linewidths of these peaks make this experiment less than optimal for the present study.[55] Instead, to study these correlations we use a simple, but novel, adaptation of the triple-resonance experiment (Triple), which combines two different NMR frequencies, a fixed pump frequency and a variable probe frequency.[55,59] Pulsed difference Triple spectra were obtained by collecting a Davies ENDOR spectrum with only the randomly hopped probe rf pulse and then subtracting this reference spectrum from a Davies Triple spectrum obtained with *both* fixed pump rf pulse and randomly hopped probe pulse, under otherwise identical conditions. CW difference Triple spectra were collected analogously.

We have observed that both pulsed randomly hopped Triple and CW stochastic difference Triple behave similarly. When nuclear relaxation is slow, the presence of a pump rf pulse applied to a $\nu_{+/-}$ ENDOR (NMR) transition from a specific site causes an *increase* in intensity of the probe-induced, correlated (hyperfine-coupled) $\nu_{-/+}$ partner relative to a background ENDOR spectrum (no pump) taken under the same conditions. Upon taking the difference Triple (Pump on − Pump off) spectrum, a sharp decrease in intensity is observed at the pump frequency and a correspondingly sharp increase in intensity is observed at $\pm 2\nu(^{57}Fe)$, depending on whether the pumped transition is $\nu_{-/+}$. Of particular importance, this single-center correlation is highly resolved, unlike difference Triple effects that involve two *different* ^{57}Fe ENDOR centers, which exhibit orientation-selective broadening.[60] These two-center effects typically are used to determine the relative signs of hyperfine couplings,[55,59] but in the slow-relaxation regime and in particular with the highly overlapped spectra displayed here, this approach is superseded by absolute sign determinations discussed below. Figures S3 and S4 (Supporing Information [SI]) exhibit CW (S3) and pulsed (S4) difference Triple spectra for ^{57}Fe peaks whose correlation is independently established by their separation of $2\nu(^{57}Fe)$.

This increase in intensity of a correlated partner under conditions of slow relaxation is opposite in sign from the response in a difference Triple spectrum taken when nuclear relaxation is rapid. In that case, peaks arising from transition in the manifold opposite the pumped transition show no change in intensity and peaks associated with transitions in the same manifold as the pumped transition show decreases in intensity.[61,55,62]

Hyperfine Sign Determination. Signs of the hyperfine couplings measured from ENDOR spectra (more precisely, the sign of A/g_N) were obtained by the recently developed Pulse-Endor-SaTuration and REcovery (PESTRE) multisequence protocol.[41] This employs a pulse sequence comprised of multiple Davies ENDOR sequences, carried out in three distinct experimental stages: (I) an EPR saturation stage (rf off) typically consisting of 100 Davies sequences whose spin−echo intensities quickly converge to the steady-state 'baseline' (*BSL*); (II) an ENDOR perturbation stage of 24 sequences, in which each sequence contains a fixed rf set at one or the other of the branches of the ENDOR spectrum; and (III) an EPR recovery stage (rf off) of up to 388 sequences during which the spin echo corresponds to the spin−echo 'dynamic reference level' (*DRL*) associated with ENDOR-induced spin polarization created in the second stage, with the *DRL* relaxing to the *BSL* during this stage. In the slow-relaxation regime,[63] the sign of A is unambiguously given by the sign of the difference between the *DRL* and *BSL* echo intensities, denoted as *DRL*δ, a *single* ENDOR branch, *either* ν_+ or ν_-.[41,42] The exact time-dependent solution[41] of the master

equation[64,65] for the electron/nuclear spin populations after each Davies pulse sequence in a multipulse sequence shows the following properties: when $A > 0$ (and $g_N > 0$ as with ^{57}Fe), if ν_+ is being interrogated, the *DRLδ* is negative, and the trace *DRL* exhibits a slow rise to the *BSL*; when ν_- is being interrogated, the *DRLδ* is positive, and the *DRL* exhibits a slow fall to the *BSL* When $A < 0$, the opposite behavior is observed.

In addition to the multisequence PESTRE protocol, a modified procedure, denoted RD-PESTRE (Raw-Data PESTRE) was applied.[66] An RD-PESTRE spectrum gives the equivalent of a simultaneous readout of the differences between the *DRL* and *BSL* at the beginning of stage III of a standard PESTRE trace across the ENDOR spectrum, and thus can be interpreted in terms of the signs of hyperfine couplings. An RD-PESTRE spectrum therefore corresponds to the combination of results from numerous single-frequency PESTRE traces collected across the ENDOR spectrum. This technique involves the collection of multiple (n_s) random-hop Davies ENDOR scans by recording the electron spin echo (ESE) for each individual rf frequency within each spectrum, rather than summing the responses at each frequency 'on the fly', to generate one large a raw data set comprised of [rf frequency, ESE response] pairs. A standard ENDOR spectrum is obtained from such a data record by a postprocessing decoding in which the ESE at each specific rf frequency is summed over all n_s spectra.

The RD-PESTRE spectrum is obtained by a more complicated postprocessing protocol. The RD-PESTRE response for a specific frequency, ν_k, is obtained by examining the difference between the ESE of the transient that immediately follows ν_k within each scan (denoted, ν_r) and the *average* value of the ESE transient at ν_r over the entire data set. This average 'instantaneous deviation' is a measure of the influence that the transition at ν_k has on the *DRL* of the following transient. The instantaneous deviations for a each value of ν_k are summed across the entire data set to produce a spectrum that is related to $DRL\delta(\nu_k)$. In order for this *DRLδ* spectrum to be used in hyperfine determination, it must be compared to an equivalent of the baseline signal level. As this equivalent, we generate a spectrum $Null(\nu_k)$ by a similar procedure where $Null(\nu_k)$ is defined by the sum of the instantaneous deviations for the ESE transients that precede, rather than follow, ν_k. The signs of the response of the $DRL\delta(\nu_k)$ relative to $Null(\nu_k)$ give the same information as the sign of the difference between the *DRL* and *BSL* of a PESTRE trace, and thus the RD-PESTRE spectrum allows a readout of the signs of all hyperfine couplings for which the *DRLδ* is nonzero.

RESULTS

35 GHz EPR Spectroscopy. Resting state wild-type (WT) MoFe protein (E_0) shows a rhombic EPR spectrum from $S = 3/2$ FeMo-co that is conventionally treated in terms of a fictitious spin $S' = 1/2$ with **g**-tensor, $\mathbf{g}' = [4.32, 3.64, 2.0]$. The EPR spectrum of α-70^{Ile} MoFe in its E_0 state shows two $S = 3/2$ signals: one with $g_1(a)' = 4.36$ ($S' = 1/2$), which corresponds to the signal for WT enzyme, and another with a slightly higher value, $g_1(b)' = 4.53$. These signals have been assigned to alternate conformations of amino acids near FeMo-co.[29] The temperature and microwave power dependences of the $S = 3/2$ EPR signals from α-70^{Ile} MoFe protein as observed both by CW and pulsed (ESE) EPR methods are very similar to those of WT enzyme. When the α-70^{Ile} MoFe protein is freeze-trapped during H^+ reduction under Ar, the majority of its E_0 EPR signal likewise disappears, but it is replaced by the $S = 1/2$ signal, $\mathbf{g} = [2.16, 2.01, 1.97]$, of the E_4 MoFe state.[3,35] These 35 GHz CW EPR signals are shown in Figure S1 (SI).

CW 35 GHz ENDOR Spectroscopy. The 35 GHz CW ENDOR spectra of ^{57}Fe-enriched α-70^{Ile} MoFe protein exhibit signals from strongly coupled ^{1}H that span a range of as much as ~30 MHz, centered at the proton Larmor frequency ($\nu_H \approx 50$ MHz); previously these have been fully analyzed and assigned to the bound hydride(s).[30] These signals do not change upon ^{57}Fe enrichment. In the lower radio frequency range (<25 MHz), both CW and pulsed ENDOR spectra of the natural-abundance (^{56}Fe) intermediate are essentially featureless, while the isotopically enriched cofactor shows multiple, intense ^{57}Fe signals.

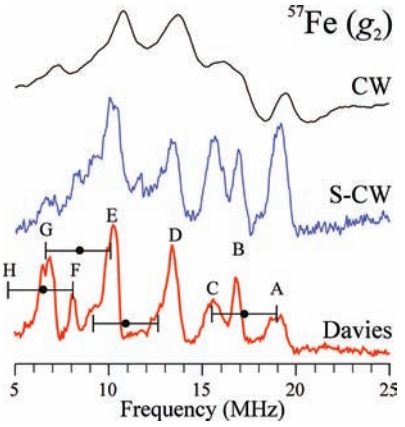

Figure 2. The 35 GHz CW (top), stochastic CW (middle), and random-hop Davies pulsed (bottom) ^{57}Fe ENDOR spectra collected at $g_{2(mid)}$ for the E_4 intermediate of the α-70^{Ile} variant of Mo^{57}Fe protein nitrogenase intermediate trapped under Ar (proton) turnover conditions. The "goalposts" indicate $2\nu(^{57}Fe)$ at $g_{2(mid)}$ (2.01) = 3.43 MHz. The ^{57}Fe ENDOR peaks are labeled in the Davies spectrum A−H, as described in the text. Experimental conditions: CW: microwave frequency, 35.065 GHz; temperature, 2 K; microwave power, 0.2 μW; 100 kHz field modulation amplitude, 0.3 mT; rf scan rate, +1 MHz/s; time constant, 64 ms; 50 scans; stochastic CW: as in C, but with no time constant and random "hopping" of rf in the cycle: rf on, 1.0 ms; rf off, 1.0 ms, digitizing time 1.0 ms; random-hop Davies pulsed: microwave frequency, 34.81 GHz, microwave pulse lengths, 80 ns, 40 ns, 80 ns, τ = 600 ns, T_{rf} = 35 μs; 256 frequency points/scan; repetition time, 100 ms; 50 scans, acquisition time 43 min.

As will be discussed in more detail below, electron-spin relaxation in E_4 is slow and electron−nuclear cross-relaxation is extremely slow. The latter, in particular, causes CW (Figure 2, top) *and* Davies pulsed ^{57}Fe ENDOR spectra (not shown) to have limited resolution when the rf is 'swept' continuously from high-low frequency or the reverse. In addition, in the 'rapid-passage' regime that characterizes CW EPR and ENDOR spectra at 2 K, the CW ENDOR spectra are slightly 'offset' in the direction of the sweep (Figure 2) and are extremely sensitive to the EPR field modulation amplitude (Figure S2 [SI]). With extreme care, these difficulties can be managed so as to allow selected features to be followed across the EPR envelope. This procedure was the foundation for our previous analyses of ^{57}Fe ENDOR spectra of the CO-inhibited and ethylene-bound nitrogenase intermediates.[67,68] However, we have now found that the difficulty is overcome by collecting the CW or Davies pulsed ENDOR spectra respectively with 'stochastic'[54] and 'random-hop'[56] selection of the frequencies within the desired range (Figure 2, middle and bottom, respectively). Of these two implementations of the stochastic approach,[54] the pulsed version also allows us to use PESTRE to determine the signs of the ^{57}Fe hyperfine couplings, so we focus on these measurements.

Random-hop Davies pulsed (and stochastic CW) ENDOR spectra collected at g_2 (Figure 2) show eight resolved peaks (denoted A−H in descending frequency). As shown in the

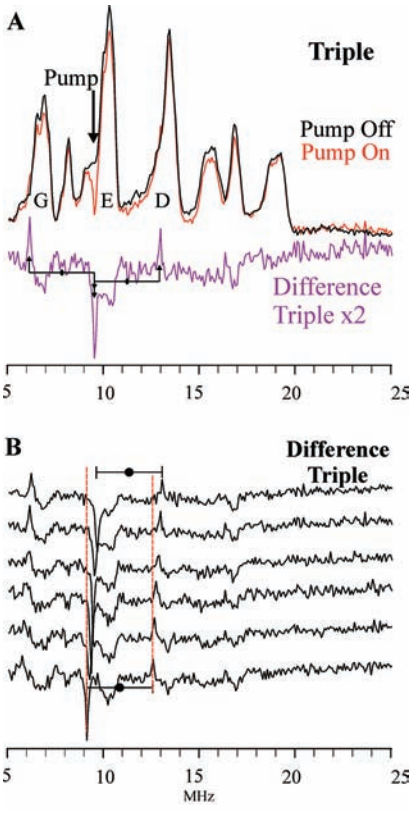

Figure 3. (A) **Top**: Random-hopped Davies ENDOR spectra recorded at g_2 (12390 G, 34.80 GHz) with an rf pump at 9.60 MHz, as indicated by arrow (red spectrum), and without the pump (black). **Bottom**: Difference Triple response (×2) obtained by simple subtraction, (Pump on − Pump off). The two positive spikes at 6.2 and 13.0 MHz demonstrate that intensity at 9.60 MHz is tied to two different ^{57}Fe centers, one with $|A/2| = 7.9$ MHz and the other with $|A/2| = 11.3$ MHz, as shown by the goalposts. Although other correlations could be used to discuss relative hyperfine signs, e.g. difference peaks B,C/G/E, in each case those peaks involve overlapped intensity and so relative signs are not unambiguously determined. *Conditions*: repetition time 50 ms, rf pulse lengths 25 μs, acquisition time 43 min for each spectrum. All other conditions are as in Figure 4. (B) Difference Triple spectra taken as the pump frequency is stepped by 0.1 MHz from 9.6 to 9.1 MHz. Dotted red verticals are there to guide the eye. *Conditions:* As in (A) except repetition time.

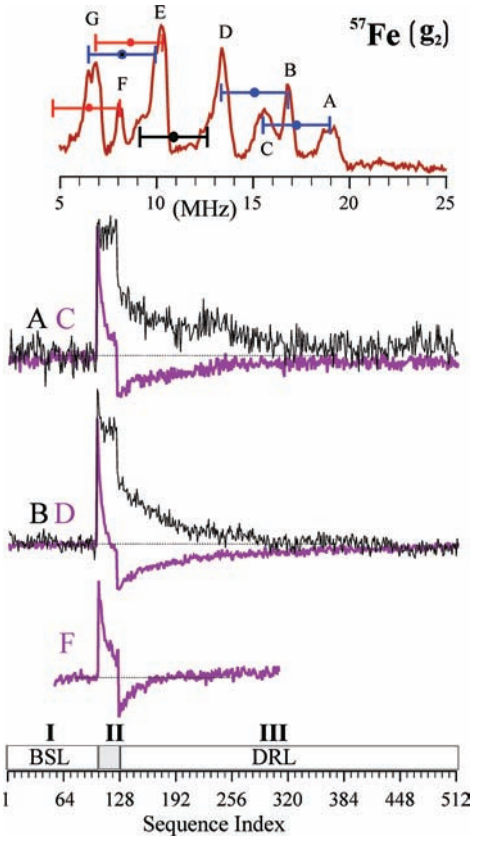

Figure 4. Determination of signs of hyperfine couplings at g_2 by PESTRE technique. **Top**: Davies ENDOR spectrum indicating the ENDOR peaks being interrogated. The goalposts here are color coded to indicate sign of hyperfine coupling: blue, negative; red, positive; black, undetermined. **Center**: PESTRE traces, presented as the difference between the observed ESE signal and the BSL (Δ*ESE*) recorded at: upper set: peaks A (black trace) and C (purple trace); middle set: B (black trace) and D (purple trace); lower: F (purple trace). **Bottom**: schematic of the PESTRE protocol showing Stage I (rf off, *BSL*); Stage II (rf on, ENDOR signal); Stage III (rf off, *DRL*). PESTRE conditions: microwave frequency, 34.81 GHz; microwave pulse lengths, 120 ns, 60 ns, 120 ns; τ = 600 ns; rf pulse length, 25 μs; repetition time 100 ms; acquisition time 17 min.

figure, by simply 'walking through' the spectrum from high to low frequency and assigning partners on the basis of the separation of the peaks within a ν_+/ν_- pair, $2\nu(^{57}\text{Fe}) \approx 3.4$ MHz, the peaks are readily assigned in pairs to four distinct classes of ^{57}Fe site: A−C, B−D, E−G, and F−H. Further insights into these assignments are obtained with the PESTRE technique, as discussed below. The A−C and B−D assignments also were confirmed by pulsed Triple measurements in which an rf 'pump' is applied to one peak and the response by its partner confirms the pairing (Figures S3,S4 [SI]).

Peaks D and E, though separated by $2\nu(^{57}\text{Fe})$ are not a ν_+/ν_- pair. However, both exhibit shoulders on their low rf sides that are separated by $2\nu(^{57}\text{Fe})$, and this pair of features might represent a ν_+/ν_- pair associated with an additional ^{57}Fe center. To test this possibility, pulsed Triple experiments were performed. As shown in Figure 3A, when the putative ν_- shoulder on E is pumped with an rf pulse at 9.60 MHz during a Davies random-hop ENDOR sequence and the resulting spectrum compared to the reference (no pump) ENDOR spectrum, the difference Triple spectrum (Pump on − Pump off) exhibits the expected sharp decrease in intensity ('hole') at the pump frequency along with *two* sharp increases in intensity ('spikes') at 6.2 and 13.0 MHz, exactly ∓ 3.4 MHz = $\mp 2\nu(^{57}\text{Fe})$ from the pump frequency. The spike at 6.2 MHz and hole at 9.6 MHz represent intensity from a ν_-/ν_+ pair, and together show that the E shoulder contains the expected contribution from the ν_+ branch of the ^{57}Fe doublet, centered at half the hyperfine coupling, $|A|/2 = 7.9$ MHz, which can be assigned to the E−G site noted in Figure 2. However, the hole at 9.6 MHz and spike at 13.0 MHz represent ν_-/ν_+ intensity from an additional, *fifth* class of ^{57}Fe, whose signal indeed contributes to the E−D shoulders and is centered at $|A/2| \sim 11$ MHz. Figure S5 (SI) shows that the Triple spectrum taken upon pumping either the E or the D shoulder gives the expected enhancement at the other, as expected for a ν_-/ν_+ pair.

To confirm this assignment and to examine the breadth of the ENDOR responses associated with this additional ^{57}Fe center, a suite of difference Triple experiments were obtained by lowering

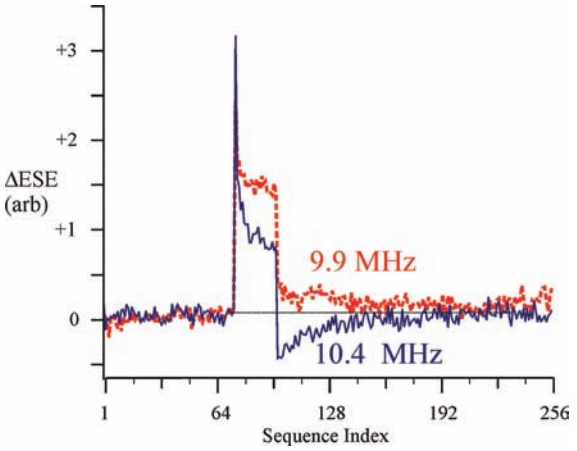

Figure 5. ΔESE PESTRE traces recorded at two frequencies on peak E (see Figure 3, top), showing the two components, E1 (blue trace, recorded at 9.9 MHz) and E2 (red trace, recorded at 10.4 MHz). PESTRE conditions as in Figure 4.

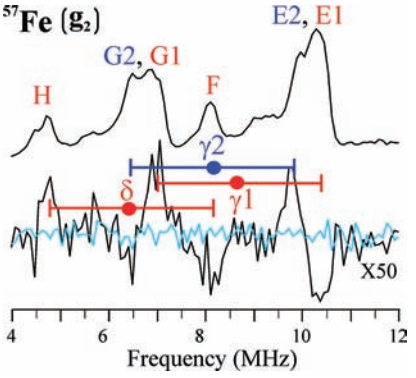

Figure 6. Determination of signs of hyperfine couplings at g_2 by RD-PESTRE technique. **Top**: expanded random-hop Davies pulsed ENDOR spectrum recorded at g_2 showing peaks E−H. **Bottom**: *DRLδ* spectrum across this ENDOR region (black trace); *Null* trace (cyan). The intensities of the two RD-PESTRE spectra have been expanded by 50-fold relative to the ENDOR trace. The goalposts are defined as in Figure 4 and here identify Fe sites δ, $\gamma1$, and $\gamma2$; the colors indicate hyperfine sign as in Figure 4. ENDOR, RD-PESTRE random-hop Davies pulsed conditions: microwave frequency 34.81 GHz; microwave pulse lengths, 120 ns, 60 ns, 120 ns; τ = 600 ns, T_{rf} = 35 μs; repetition time, 200 ms; 100 points/scan; acquisition time, 126 min.

the pump frequency by 0.1 MHz steps from 9.6 MHz (Figure 3B, top) to 9.1 MHz (Figure 3B, bottom). The suite was restricted to this range because to lower frequencies the intensity of the shoulder becomes vanishingly small; whereas to higher frequencies, Triple responses from the main peak (E) overwhelm the small contributions from the fifth site. The correlation between the pump and the ν_+ transition at (pump + 3.4 MHz) is maintained across the entire 9.6−9.1 MHz range for the pump, whereas the response to the pump at (pump − 3.4 MHz) becomes less pronounced as the pump frequency is decreased. This suite of Triple spectra thus establishes that the E−D shoulders indeed represent the fifth type of ^{57}Fe site to be detected.

The hyperfine couplings associated with all five of the ^{57}Fe classes thus far identified fall within the range 13 MHz < $|A(g_2)|$ < 34 MHz. Subsequently, these different classes of ^{57}Fe are denoted by Greek letters, beginning with α for that with the largest coupling [A−C]. The symbols, α-δ are used below for sites unambiguously characterized by ENDOR and PESTRE measurements; the symbol κ is used for the site identified by the ENDOR and difference Triple experiment given above; λ denotes an additional Fe site characterized by sum-rule arguments described below.

Signs of Hyperfine Coupling from PESTRE (pulsed ENDOR saturation and recovery). The absolute signs of the ^{57}Fe hyperfine couplings observed at g_2 were determined by application of the PESTRE technique,[41] in which the sign is determined by monitoring the response of the electron−nuclear spin system to multiple Davies sequences at fixed rf frequency (see Materials and Methods). Figure 4 shows the ΔESE = (ESE − *BSL*) traces obtained for PESTRE 'three-stage' multisequences for three classes of ^{57}Fe: the ν_+/ν_- partners, [A−C; upper pair of traces] and [B−D; middle pair of traces], and the ν_+ peak, [F (ν_- partner, H not shown); lower trace]. Figure 5 shows PESTRE sequences associated with ν_+ 'peak' [E (ν_- partner, not shown)].

As seen in Figure 4, for *both* the A−C (denoted, Feα) and B−D (Feβ) pairs, the *DRLδ* of the ν_+ partner is positive and falls to the *BSL* in stage III, and the *DRLδ* for the ν_- partner is negative. This establishes[41] that $A(^{57}\text{Fe}) < 0$ for *both* Feα and Feβ sites. This assignment would be expected by analogy with the previous studies,[67,68] but in those cases the signs were inferred by arguments discussed below and not determined experimentally; this is the first *direct* experimental evidence for the signs of ^{57}Fe hyperfine coupling in a nitrogenase intermediate. In contrast, for the ν_+ peak F of site Feδ, in stage III the *DRLδ* is negative and rises to the *BSL*, establishing that $A(^{57}\text{Fe}\delta) > 0$.

The application of PESTRE to peak E of the [E−G] 'pair' led to a surprise, as shown in Figure 5. While collecting PESTRE traces at multiple rf values across the ENDOR spectrum at g_2, it was found that the PESTRE trace recorded at the high-rf side of peak E (10.4 MHz) shows a negative *DRLδ*; hence, $A_{Fe} > 0$ for a signal denoted E1, but the trace recorded at the low-rf side of peak E (9.9 MHz) shows a positive *DRLδ*; hence, $A_{Fe} < 0$ for a signal denoted E2.

The PESTRE measurements in fact were inspired by observation with a newly developed PESTRE protocol, denoted RD-PESTRE. This technique yields a spectrum that is the equivalent to the *DRLδ* recorded across the entire ENDOR spectrum. This RD-PESTRE spectrum requires substantially more transients per point (usually 2−3×) than would be required for a simple ENDOR spectrum due to its inherently lower signal to noise ratio (S/N), but does provide a complete record of the signs of the hyperfine interactions across the ENDOR spectrum. When applied to the entire ^{57}Fe Davies spectrum at g_2 (5−25 MHz; Figure S6 [SI]), it clearly shows *DRLδ* as positive for peaks A and B and negative for C and D, in agreement with Figure 4. An expanded view of the low-frequency region, (4−12 MHz; Figure 6), shows *DRLδ* to be negative for F (in agreement with Figure 4) and positive for H, as expected for this pair (Feδ). Most importantly, Figure 6 shows derivative-shaped features for both E and G, most clearly for the more intense signal, E. These arise from the summation of positive and negative *DRLδ* from signals associated with oppositely signed hyperfine coupling constants where the differences in $|A|$ roughly equal the widths of the individual lines. This result confirms that what appears to be an [E−G] pair is actually the summation of [E1−G1] and [E2−G2] pairs that are the ν_+/ν_- partners of two distinct ^{57}Fe sites, now denoted $\gamma1$ and $\gamma2$, whose hyperfine couplings are almost identical in magnitude, but with opposite signs.

Thus, for the E_4 intermediate trapped during turnover of the α-70^{Ile} MoFe protein, six Fe sites, not merely five, of FeMo-co

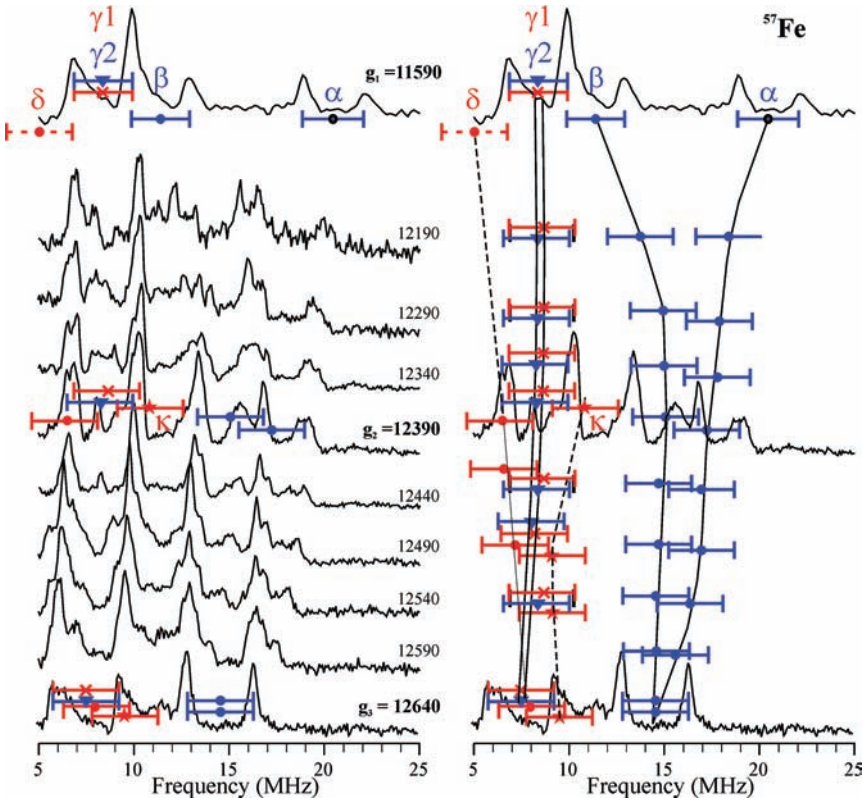

Figure 7. Two-dimensional field-frequency pattern of 35 GHz random-hop pulsed Davies ENDOR spectra. (Left) Experimental spectra with magnetic field of observation indicated. 'Goalposts' (defined as in Figure 4) indicate ν_+/ν_- doublets from the individual Fe sites, split by $2\nu(^{57}\text{Fe})$ ($\sim$ 3.4–3.5 MHz, depending on field) and are presented for canonical g-values (g_1, g_2, and g_3); sites Feα, Feβ, Feγ1, Feγ2, Feδ are identified at g_1. An additional site, Feκ, is also indicated at $g_{2(\text{mid})}$. (Right) Spectra at canonical g-values are reproduced for clarity, while the goal-posts for each well-defined doublet are presented for all spectra. For the four sites whose field dependence is clear over the full spectrum (Feα, Feβ, Feγ1, Feγ2), black lines connect the goalposts. For the other two identified sites (Feδ, Feκ), the proposed field dependence is indicated by a dashed black line. Experimental conditions as in Figure 2 (bottom).

have been identified unequivocally. The signs as well as the magnitudes of the ^{57}Fe hyperfine coupling constants have been determined for five Fe sites. RD-PESTRE measurements on the ν_- shoulder of Feκ are compatible with $A > 0$, but because this shoulder is associated with a much more intense peak (D) that has the same sign of RD-PESTRE response, the experimental sign determination for Feκ is not considered to be definitive.

Two Dimensional Field-Frequency Patterns. Davies ^{57}Fe ENDOR spectra were recorded across the entire EPR envelope of this nitrogenase intermediate, with selected spectra shown in Figure 7. As illustrated in the figure, the main features from four of the ^{57}Fe can be readily followed across the EPR envelope: α, β, and the γ1, γ2 pair. ^{57}Feα has the largest hyperfine coupling at all fields; its hyperfine interaction shows noticeable anisotropy, with A increasing progressively from low to high g value. However, its absolute anisotropy, $[(A_{\max} - A_{\min})/A_{\text{avg}}; A_{\text{avg}} = (A_{\max} + A_{\min})/2]$, is rather small. ^{57}Feβ also shows noticeable anisotropy with $|A|$ decreasing from g_2 toward g_1, but the absolute anisotropy is smaller still. The doublet associated with the γ1, γ2 pair shows minimal shift with field, with the signals from the two sites remaining overlapped throughout the pattern. Thus, these two sites have essentially isotropic hyperfine couplings that have opposite signs but differ in magnitude by less than their linewidths. The signals for ^{57}Feδ cannot be followed throughout the field, and our best suggestion as to its variation is indicated on the figure. Finally, Figure 7 shows possible assignments of features observed in the high-field (low g) region for the sixth site, ^{57}Feκ. Table 1 lists the isotropic coupling constants calculated or estimated for the six ^{57}Fe sites on the basis of the assumption that **A** and **g** are collinear, along with the full hyperfine tensors for Feα and Feβ. Given the small absolute anisotropies for the signals with large couplings and the smaller couplings for the others, the assumption of collinearity has negligible impact on the tabulated values, and thus for the discussions below, where we make use of the experimental hyperfine couplings.

Estimates of a_i for the Unresolved Fe Site. The experimental isotropic hyperfine coupling to the ^{57}Fe nucleus of site i, a_i, within a multinuclear spin-coupled cluster is proportional to the isotropic nuclear hyperfine coupling for the uncoupled Fe ion, a_i^{un} (i.e., its intrinsic isotropic coupling), with the projection of the total spin onto that local spin (K_i) as a scaling factor, with the projection factors subject to a normalization factor;[43]

$$a_i = K_i a_i^{\text{un}}; \sum_{i=1}^{n} K_i = 1 \qquad (3)$$

We shall omit the contribution of the Mo site to this sum, based on recent ^{95,97}Mo ENDOR studies of the E_4 turnover intermediate,[34] which show that spin population of the Mo site is very small, as in the resting state,[69] so we take $n = 7$ Fe sites in the summation of eq 3. The a_i^{un} for all Fe sites are negative,[70] so Fe sites with $a_i < 0$ as determined by PESTRE have $K_i > 0$, while sites

Table 1. ^{57}Fe Isotropic Hyperfine Couplings (a_i) for FeMo-co of Nitrogenase Intermediates and Resting State

	E_4[a]	S_{EPR1}[e]	lo-CO[f]	M^{Ng}
α	−35(1)	−33	−31	−18
β	−27(1)	−32	−30	−17.1
$\gamma 1$	+17(1)	−23] −26	−17	−11.8
$\gamma 2$	−16(2)	+18 (×4)	+16 (×4)	+11.7
δ	+13(2)			+11.7
κ	∼+20[c]			+9.3
λ	[+15 ⇔ 0][d]			−3.7
a_{test}[b]	−15 ⇔ −30	−17.5	−14	−17.9

[a] Determined in this work through ENDOR, PESTRE, and Triple measurements with exceptions noted in table footnotes (*c*, *d*). Estimated uncertainties in parentheses. Estimated hyperfine tensor components: Feα, $A = -[41, 34, 29]$ MHz; Feβ, $A = -[23, 30, 29]$ MHz; Fe(1, Fe(2, essentially isotropic; others, not determined. [b] The sum of the seven individual a_i values corresponds to a_{test} (see eqs 3 and 4).[70] [c] Magnitude obtained from ENDOR; sign obtained through use of eq 4 (see text). [d] Calculated from other tabulated a_i through use of eq 5 (see text). [e] Intermediate that contains a complex of FeMo-co with C_2H_4, the reduction product of C_2H_2.[28] [f] Intermediate that contains a complex of FeMo-co with one CO.[79] [g] Resting-state FeMo-co.[19]

with positive coupling have $K_i < 0$. The isotropic coupling for Feλ, which has not been characterized by ENDOR, can be estimated by employing the parameter a_{test}, defined as follows,[43]

$$a_{test} = \sum_{i=1}^{7} a_i \quad (4)$$

Upon adopting a value for a_{test}, one can use this equation to corroborate the sign of a_κ and obtain an estimate for a_λ. Then, by using the signed values for a_κ and the other five resolved couplings one can estimate a_λ:

$$a_\lambda = a_{test} - \sum_{i=1}^{6} a_i \quad (5)$$

For resting state, WT FeMo-co,[19] $a_{test} = -17.9$ MHz. The values compiled by Mouesca et al.[43] include $a_{test} = -21(3)$ MHz for FeS systems such as 1Fe (rubredoxin), and most $[Fe_4S_4]^{1-}$ and $[Fe_3S_4]^{0,1+}$ clusters. Lacking specific knowledge as to the value of a_{test} for the FeMoco in the Ar turnover state studied here, we consider the plausible range, $-15 \gtrsim a_{test} \gtrsim -25$ MHz, although the results for resting-state FeMo-co suggest the middle of this range is the more likely.[71]

In using eq 4 to examine the sign of a_κ and estimate a_λ, several constraints have been applied. First, examination of Figure 7 leads to the conclusion that the uncharacterized ^{57}Feλ site must have $|a_\lambda| \lesssim 20$ MHz for its signal to be undetected at any field of observation: the higher-frequency range is relatively uncrowded, and high-frequency ENDOR signals are generally easily detected. In contrast, the congestion in the lower-frequency range could easily hide the unidentified signal(s). Second, consideration of eqs 2, 3 shows that neither of the sites with the two largest couplings, Feα and Feβ, can be associated with two equivalent ^{57}Fe sites, independent of whether they have the same sign for a_i or opposite signs. If such a pairing did occur for Feα and/or Feβ, then eq 4 would require an unacceptable value for a_{test}. Upon application of these constraints, calculations with eqs 4 and 5 confirm that $a_\kappa > 0$ (Table 1). Then the six experimentally determined a_i (Table 1) are inserted in eq 5, and assignment of a value of a_{test} yields an estimate of a_λ. The value $a_{test} \approx -25$ MHz, toward the upper magnitude end of the plausible range, gives $a_\lambda \approx 0$, which would be unobservable; for $a_{test} \approx -15$ MHz, toward the lower magnitude end of the range, $a_\lambda \approx +15$ MHz, which would be observable in principle but likely obscured by Feδ. This whole range of a_λ thus satisfies the constraint, $|a_\lambda| \lesssim 20$ MHz, while predicting that the signals from Feλ be either unobservable or fall within an extremely congested region of the spectrum, thereby explaining the inability to identify the responses from this site. Table 1 summarizes the final results for the isotropic couplings for the seven Fe sites of FeMo-co in the E_4 intermediate as determined in this work.

In our earlier ^{57}Fe ENDOR studies of nitrogenase intermediates we used the isotropic hyperfine couplings to analyze the metal-ion valencies of individual Fe sites by approximating $a_i^{un} \approx a_{test}$ and using eq 3 to calculate K_i values for the best available choice for a_{test}. However, given that a_{test} is not narrowly constrained and recent computations suggest that the Fe sites may exhibit a range of a_i^{un}, we suggest that such an analysis for E_4 would be premature. Nonetheless, for reference, Table S1(SI) contains a set of K_i values calculated from the isotropic couplings presented in Table 1 under the assumption that $a_{test} = -19$ MHz, the resting state value.

DISCUSSION

This report presents highly resolved 35 GHz ^{57}Fe random-hop Davies ENDOR spectra from FeMo-co of the E_4 state of the α-$70^{Val\rightarrow Ile}$ MoFe protein, the state that was shown by a step-annealing protocol to have been optimally activated for binding and reduction of N_2 through the accumulation of $n = 4$ electrons.[35] In combination with the newly developed PESTRE protocol for determining the signs of hyperfine couplings, we have determined the signed isotropic hyperfine couplings for five of the seven iron sites of the reductively activated E_4 FeMo-co, while the Triple technique has given the magnitude of the coupling for a sixth. Supplemental use of the a_{test} sum-rule enabled us to estimate the signed isotropic coupling for the remaining iron site, Table 1. Together with recent ^{95}Mo ENDOR measurements on E_4,[34] this yields hyperfine couplings for all the metal sites of FeMo-co in E_4.

^{57}Fe Characteristics of E_4. The first key experimental finding is that the two most-strongly coupled Fe sites both have negative hyperfine couplings, corresponding to $K_i > 0$, as was in fact inferred from the a_{test} sum-rule for the lo-CO and S_{EPR1} (C_2H_4 bound) intermediates in the absence of direct determination of hyperfine signs. In contrast, the relatively small isotropic coupling for Feγ is positive, corresponding to $K_\delta < 0$. The most surprising finding is that the E−G pair of features in the g_2 ^{57}Fe ENDOR spectrum of E_4 (Figure 2) corresponds to two Fe sites, $\gamma 1$ and $\gamma 2$, with coupling of almost identical magnitude but opposite signs, Figures 5, 6; the full field dependence of the ^{57}Fe pattern (Figure 7) further establishes that the hyperfine interactions for the two Feσ sites are almost completely isotropic; although the isotropic couplings for $\gamma 1$ and $\gamma 2$ are opposite in sign, they have the same magnitude within a few percent. Table 1 contains the signed isotropic couplings for the six experimentally characterized Fe sites, α-δ, κ. It further includes the range of values for Feλ derived from the a_{test} sum-rule for the plausible range of values of a_{test}.

Electron Inventory. The combination of the results of the ^{1}H ENDOR and step-annealing studies of E_4 further allows us to determine the redox state of the metal-ion core of E_4 FeMo-co

through evaluation of the 'electron inventory'[28] of the E_4 state in a way that has not been possible for any intermediate previously. Consider a MoFe protein intermediate, E_n, that has accumulated n electrons beyond the electron count of the resting state ($n = 0$; denoted E_0). In an electron inventory, the number of those n electrons that are associated with the metal ions of FeMo-co itself is denoted m, the number that have been transferred to substrate is denoted s; in addition, the P cluster may have been oxidized by a number of electrons, p, with these electrons having been transferred to FeMo-co. These individual elements in the inventory can be combined into a simple expression for the total number of electrons that have been added to the metal ions of FeMo-co in the E_n state, relative to the number on the resting state: $m = n - s + p$. One may finally partition the m electrons residing on FeMo-co into $m = f + o$, where f is the number of electrons used for reduction of Fe ions and o the number of electrons by which Mo(IV) of resting state has been reduced.

The MoFe protein in the state studied here was shown to have accumulated $n = 4$ electrons through the finding that in the frozen state at −20 °C it relaxes to the resting state in two stages, each of which is accompanied by the loss of H_2, hence the notation E_4. As in all intermediate states studied to date, E_4 exhibits no EPR signal from oxidized P cluster, and thus $p = 0$. Recent ^{95}Mo ENDOR studies indicate that the redox level of the Mo ion is unchanged between resting state and E_4, so $o = 0$ and $m = f$.[34] As a result of these considerations, the E_4 inventory is particularly simple: $m = f = n - s = 4 - s$; the number of electrons that have been added to the Fe ions of FeMo-co equals the number added to the MoFe protein, less those that have been added to bound 'substrate'.

The number of electrons on 'substrate' for E_4, s, is unambiguous. During turnover under Ar, the only possible substrate is H^+, which is reduced to H_2. Our previous[29] ^{1}H ENDOR study of the E_4 intermediate disclosed signals from two symmetry-related ^{1}H bound to metal ion(s) of FeMo-co. Analysis of the dipolar component[29] led us to conclude that these two species are hydrides that bridge two metal ions, rather than binding terminally to a single ion. A recent ^{1}H ENDOR study of a terminal hydride bound to Mo(III) confirmed the basis of this conclusion,[42] while a ^{95}Mo ENDOR study of E_4 indicated that Mo is not involved in binding the hydrides,[34] which thus are assigned to [Fe-(μ-H$^-$)-Fe] moieties. Each of the two bridging hydrides can be thought of as having been formed by the two-electron oxidative addition of a proton to the FeMo-co core (s = 2 per proton); the two hydrides together then make a contribution to the electron inventory, $s = 4$. The step-annealing protocol that revealed the state under study here to be E_4 further showed that it has accumulated a total of four protons as well as four electrons,[22] in keeping with the LT scheme.[17,18] The third and fourth protons are not bridging hydrides and cannot have added to Fe to form terminal hydrides. On the basis of the relatively large ^{57}Fe couplings for the Fe sites (Table 1) and results for a biomimetic complex with a terminal hydride,[42] such species must give readily observable ^{1}H ENDOR signals that are distinct from those of the two bridging hydrides, contrary to experiment. Instead, FeMo-co of the E_4 state must bind two protons in addition to the two bridging hydrides through acid/base protonation of S^{2-}; whether this involves formation of a bridging (M-(μ-SH$^-$)-M′) fragment or the breaking of an Fe−S bond and formation of a terminal Fe-SH is not known.[72] For purposes of the electron inventory, these two protons contribute $s = 0$. Thus, overall, the electron inventory then includes as the number of electrons that reside on the E_4 FeMo-co metal ions, relative to the number on M^N, $m = n - s = 0$: the FeMo-co metal ions of the E_4 state trapped during turnover of the α-70$^{Val\rightarrow Ile}$ MoFe protein are formally at the same redox level as in the resting state (E_0) FeMo-co.[22−24]

The conversion of the $S = 3/2$ resting state to the $S = 1/2$ E_4 intermediate at the same redox level is not 'merely' a high-spin to low-spin conversion, such as that seen, for example, upon CO binding to Fe(II) hemes. The large hydride hyperfine interactions show that the hydrides do *not* bind to $S = 0$ Fe ion(s) (e.g., low-spin Fe(II)). Instead, it seems clear that the influence of the two bridging hydrides, in conjunction with whatever structural rearrangements may accompany the binding of two protons to sulfur, must instead induce an alteration in the spin-coupling scheme. As the metal ions are *not* highly reduced in the E_4 state by the injection of four electrons into FeMo-co—and in fact are not formally reduced at all ($m = 0$)—we may further surmise that structural rearrangements play a key role in activating FeMo-co for reactive binding of N_2. These structural changes may 'merely' include breaking of an Fe−X bond, where X is the interstitial atom found by X-ray diffraction (C, N, or O),[8] breaking of an S−Fe or S−Mo bond, or some combination of such changes.

The finding that MoFe is reduced by 4 equivalents ($n = 4$) without reduction of any FeMo-co (or P cluster) metal ion led us to reconsider previous conclusions about the state of FeMo-co in the $S = 1/2$ CO-inhibited forms of WT nitrogenase and in the $S = 1/2$ intermediate that contains the ethylene product of acetylene reduction bound to FeMo-co, denoted S_{EPR1}. For these intermediates, 35 GHz CW ^{57}Fe ENDOR was used to estimate the ^{57}Fe hyperfine coupling tensor components for multiple Fe sites,[28,44] and these results were used in an electron inventory analysis. With seven Fe sites giving overlapping signals the ENDOR analysis is a formidable task, and even a successful assignment of tensor components using conventional ENDOR does not yield the sign of the hyperfine couplings. Nonetheless, through application of the a_{test} sum-rule (eq 4), these signs were inferred without their direct experimental determination.

Consider the E_n intermediate that contains the ethylene product of acetylene reduction bound to FeMo-co, S_{EPR1}. If ethylene acts as a dative π-donor (π-C_2H_4), this binding does not alter the formal reduction level of the FeMo-co (m) or the alkene ($s = 2$), and the complex has an electron inventory, $n = m + s = m + 2$ (with $p = 0$). As in other formal valency schemes, however, the inventory depends on the nature of the binding of substrate-derived fragments to FeMo-co. Thus, one might instead imagine that C_2H_4 actually binds through C−Fe σ-bonds as the ferracyclopropane (oxidative addition of alkene to FeMo-co; σ-C_2H_4). Such a structure corresponds to oxidative addition of C_2H_4 to the FeMo-co, and in this case the alkene must be described formally as having accepted two additional electrons from FeMo-co, making a total of $s = 4$ electrons transferred to the initial C_2H_2 substrate. As a result, $n = m + 4$. Analysis of the ^{57}Fe ENDOR measurements, in combination with a variety of other considerations, led us to prefer $n = 4$ for this intermediate, compatible with the finding of Lowe et al. that C_2H_4 is released from the E_3 and E_4 states during C_2H_2 reduction by WT enzyme.[73] The similarity between the ^{57}Fe couplings now measured here for the E_4 intermediate and those previously estimated for S_{EPR1}, Table 1, strongly supports the conclusion that the metal-ion core of FeMo-co S_{EPR1}, like that of E_4, indeed remains at the formal redox level of the resting state ($m = 0$).

This interpretation thus implies that S_{EPR1} also has accumulated $n = 4$ electrons, and that the bound alkene thus forms a σ-bonded ferracyclopropane species with $s = 4$.

Redox Couples Accessed by the FeMo-co Metal-Ion Core. The similar metal-ion properties and metal-ion redox levels in intermediates formed during the reduction of such different substrates, H^+ and C_2H_2, has led us to conjecture that *in general* FeMo-co is a 'poor capacitor', and that the metal ions of FeMo-co themselves never accumulate more than one reducing equivalent. Instead, FeMo-co is a good 'battery' in that it stores accumulated reducing equivalents two-at-a-time in metal (Fe) hydride and/or hydrogenated substrate chemical bonds. According to this idea, addition of one electron may reduce the metal ions, but when a second equivalent is delivered to FeMo-co, instead of further reduction of metal ions, both electrons are 'shuttled' onto a bound substrate moiety. Stated differently, we propose that throughout the catalytic reduction of substrates, the inorganic core of FeMo-co cycles through only one redox couple composed of two formal redox states, those associated with M^N and M^R: E_n states with n even would have the metal ions at the resting-state redox level, M^N; E_n states with n odd would be in the one-electron reduced form, M^R. As needed, the formation of a metal-bound hydride would provide a means of 'storing' an accumulated pair of electrons until FeMo-co is activated sufficiently to carry out a substrate hydrogenation.

In the LT kinetic scheme for nitrogen fixation by nitrogenase, both a proton and an electron are delivered in each stage of reaction. In the most reductively activated state of the MoFe protein prior to N_2 binding, the E_4 state, FeMo-co has accumulated four reducing equivalents, the most possible without any being transferred to a 'real' substrate (N_2, C_2H_2, etc.), but the electron inventory shows that this accumulation of four e^- and H^+ leaves FeMo-co in the M^N redox state, with two μ-H^- ligands, and (presumably) two S-bound H^+ to balance the charge.[29] Correspondingly, we suggest that E_3 contains one metal hydride and two protons bound to FeMo-co with metal ions in the M^R redox level, E_2 one hydride and one proton bound to FeMo-co in the M^N state, E_1 one proton and M^R.

Once N_2 binds (to E_3 or E_4), it is progressively hydrogenated as the enzyme proceeds along the reaction pathway[74] to the formation of two NH_3 molecules. In these later stages of the pathway, the accumulation of reducing equivalents by substrate thus replaces hydride formation as a means of obviating the need for reduction of metal ions in the FeMo-co core. Indeed, one might imagine that once substrate is bound, an electron/proton delivered to FeMo-co to generate an E_n state with $n > 4$ might hydrogenate the substrate without reducing the core at all.[3]

The binding of N_2 to E_4 is thought to be accompanied by the loss of H_2 formed by combination of one of the two hydride/proton pairs, thus leaving one hydride/proton pair bound along with N_2 to what we would assign as FeMo-co in the M^N redox state. How far along the reaction pathway might the second hydride/proton pair coexist with N_2 or a partially hydrogenated nitrogenous fragment before doubly hydrogenating the substrate is a question considered in our recent discussion of electron delivery to substrate.[3]

If FeMo-co exhibits only two redox levels during catalysis, then why is it constructed from so many metal ions? Our results suggest that hydride binding and substrate reduction require a 4Fe face, and it is further likely that catalysis is modulated by the linkage of these Fe ions to a hemilabile anionic **X**, with the making and breaking of Fe−**X** bonds tuning FeMo-co reactivity through generation of coordinatively unsaturated Fe ions. The formation of such a face and the incorporation of **X** could not occur with a smaller cluster, as no less than a trigonal prism of 6 Fe ions is needed to generate these structural features. In FeMo-co, the trigonal prismatic core of 6 Fe ions plus **X** is capped, and likely 'tuned', by two ions, one Fe plus Mo, or V or Fe in the alternative nitrogenases.

The conjecture that during catalysis the eight-metal-ion core of FeMo-co employs only two redox levels—one redox couple—might seem "bold".[75] Recall, however, that the use of a single redox couple is not unusual for FeS clusters. The 4Fe clusters, which could potentially access five redox levels (four redox couples) overwhelmingly function by use of only one couple in a given protein environment, with the 4Fe-ferredoxins exhibiting the $[4Fe4S]^{2+/1+}$ couple, but HiPIPs exhibiting the $[4Fe4S]^{3+/2+}$ couple.[76]

Viewed from a broader perspective, this conjecture merely extends our long-accepted understanding of how enzymes function. In general, enzymes require a large protein construct to generate the small organized volume that constitutes the active site. It takes only a small extension of this view to suggest that the 4Fe/**X** face of FeMo-co, which appears to be required to carry out the difficult task of N_2 reduction, can be generated only as part of a structure that at minimum involves two additional Fe ions to make the trigonal prism; FeMo-co merely has two more capping metal ions. After all, Fe hydrogenase employs a total of 6 Fe ions to carry out H_2 production at a dinuclear Fe site

Aconitase provides a final, and perhaps most telling, supporting example.[77] This FeS enzyme uses only one of the Fe sites of a 4Fe cluster, without redox changes at all, to carry out dehydration/hydration reactions that one might expect to be catalyzed by a mononuclear Zn center.

Further study is of course required to test this 'single-couple' conjecture. As one avenue of investigation, an additional class of intermediate is created by turnover in the presence of inhibitors like CO. The $S = 1/2$ lo-CO intermediate was earlier shown to have ^{57}Fe characteristics similar to those of E_4 (Table 1), suggesting that this state also contains FeMo-co with metal ions at the M^N redox level ($m = 0$), but is trapped in an alternate spin-coupling scheme by the binding of CO. Indeed, we originally suggested that $m = 0$, $s = 0$, and thus $n = 0$ for lo-CO,[44] but later accepted the proposal that $n = 2$, $s = 0$, yielding $m = 2$, based on the consensus metal-ion valencies for M^N. Clearly, a reexamination of this state, including measurements of the ^{95}Mo ENDOR and DFT computations,[24,78] is in order, as the present results favor the original formulation of $m = 0$. Perhaps most important will be a study of the $S = 1/2$ intermediate formed upon turnover of WT nitrogenase with N_2 and of the common $S = 1/2$ intermediate formed upon turnover of the α-70^{Ala}/α-195^{Gln} MoFe protein with either diazene or hydrazine.[74]

We suggest further studies to test whether this conjecture extends to other complex FeS enzymes.[58]

CONCLUSIONS

The application of novel ^{57}Fe ENDOR methodologies to the E_4 state, in combination with a recent ^{95}Mo ENDOR study has yielded the hyperfine couplings to the eight metal ions of FeMo-co in this intermediate as a foundation for future theoretical investigation. An electron inventory of E_4, carried out in the context of earlier ^{1}H ENDOR studies of this state, leads to the conclusion that the inorganic, metal-ion core of FeMo-co in E_4 is

at the same redox level as resting-state FeMo-co. Comparisons to earlier ^{57}Fe ENDOR and electron inventory assessments of other intermediates inspire the conjecture that throughout the eight-electron reduction of N_2 according to eq 1, the inorganic core of FeMo-co cycles through only the single redox couple connecting two formal redox states: those associated with the resting state, M^N, and the one-electron reduced form, M^R.

■ ASSOCIATED CONTENT

Supporting Information. Additional figures illustrating the CW 35 GHz EPR spectrum of the E_4 intermediate, effects of field modulation amplitude on CW 35 GHz ^{57}Fe ENDOR, CW, and pulsed difference Triple spectra, and broad scan RD-PESTRE spectra. This material is available free of charge via the Internet at http://pubs.acs.org.

■ AUTHOR INFORMATION

Corresponding Author
bmh@northwestern.edu

Present Addresses
¶Department of Biological, Chemical and Physical Sciences, Roosevelt University, Chicago, Illinois 60605, United States

■ ACKNOWLEDGMENT

This work has been supported by the NIH (GM59087, L.C.S. and D.R.D.; HL 13531, B.M.H.) and the NSF (MCB-0316038, B.M.H.).

■ REFERENCES

(1) Burgess, B. K.; Lowe, D. J. *Chem. Rev.* **1996**, *96*, 2983.
(2) Rees, D. C.; Tezcan, F. A.; Haynes, C. A.; Walton, M. Y.; Andrade, S.; Einsle, O.; Howard, J. B. *Philos. Trans. R. Soc. London, Ser. A* **2005**, *363*, 971.
(3) Hoffman, B. M.; Dean, D. R.; Seefeldt, L. C. *Acc. Chem. Res.* **2009**, *42*, 609.
(4) Seefeldt, L. C.; Hoffman, B. M.; Dean, D. R. *Annu. Rev. Biochem.* **2009**, *78*, 701.
(5) Dos Santos, P. C.; Dean, D. R.; Hu, Y.; Ribbe, M. W. *Chem. Rev.* **2004**, *104*, 1159.
(6) Shah, V. K.; Brill, W. J. *Proc. Natl. Acad. Sci. U.S.A.* **1977**, *74*, 3249.
(7) Howard, J. B.; Rees, D. C. *Chem. Rev.* **1996**, *96*, 2965.
(8) Einsle, O.; Tezcan, F. A.; Andrade, S. L. A.; Schmid, B.; Yoshida, M.; Howard, J. B.; Rees, D. C. *Science* **2002**, *297*, 1696.
(9) Kim, J.; Rees, D. C. *Science* **1992**, *257*, 1677.
(10) Kim, J.; Rees, D. C. *Nature* **1992**, *360*, 553.
(11) Chan, M. K.; Kim, J.; Rees, D. C. *Science* **1993**, *260*, 792.
(12) Sorlie, M.; Christiansen, J.; Lemon, B. J.; Peters, J. W.; Dean, D. R.; Hales, B. J. *Biochemistry* **2001**, *40*, 1540.
(13) Fisher, K.; Dilworth, M. J.; Newton, W. E. *Biochemistry* **2000**, *39*, 15570.
(14) Chatt, J.; Dilworth, J. R.; Richards, R. L. *Chem. Rev.* **1978**, *78*, 589.
(15) Thorneley, R. N. F.; Eady, R. R.; Lowe, D. J. *Nature* **1978**, *272*, 557.
(16) Christiansen, J.; Dean, D. R.; Seefeldt, L. C. *Annu. Rev. Plant Physiol. Plant Mol. Biol.* **2001**, *52*, 269.
(17) Thorneley, R. N. F.; Lowe, D. J. In *Molybdenum Enzymes*; Spiro, T. G., Ed.; Wiley-Interscience: New York, 1985; Vol. 7, p 89.
(18) Wilson, P. E.; Nyborg, A. C.; Watt, G. D. *Biophys. Chem.* **2001**, *91*, 281.
(19) Yoo, S. J.; Angove, H. C.; Papaefthymiou, V.; Burgess, B. K.; Muenck, E. *J. Am. Chem. Soc.* **2000**, *122*, 4926.
(20) True, A. E.; Nelson, M. J.; Venters, R. A.; Orme-Johnson, W. H.; Hoffman, B. M. *J. Am. Chem. Soc.* **1988**, *110*, 1935.
(21) Hoffman, B. M.; Roberts, J. E.; Orme-Johnson, W. H. *J. Am. Chem. Soc.* **1982**, *104*, 860.
(22) Lukoyanov, D.; Pelmenschikov, V.; Maeser, N.; Laryukhin, M.; Yang, T. C.; Noodleman, L.; Dean, D.; Case, D.; Seefeldt, L.; Hoffman, B. M. *Inorg. Chem.* **2007**, *46*, 11437.
(23) Lovell, T.; Liu, T.; Case, D. A.; Noodleman, L. *J. Am. Chem. Soc.* **2003**, *125*, 8377.
(24) Pelmenschikov, V.; Case, D. A.; Noodleman, L. *Inorg. Chem.* **2008**, *47*, 6162.
(25) Dos Santos, P. C.; Igarashi, R. Y.; Lee, H.-I.; Hoffman, B. M.; Seefeldt, L. C.; Dean, D. R. *Acc. Chem. Res.* **2005**, *38*, 208.
(26) Seefeldt, L. C.; Dean, D. R.; Hoffman, B. M.; Dos Santos, P. C.; Barney, B. M.; Lee, H.-I. *Dalton Trans.* **2006**, 2277.
(27) Lee, H.-I.; Igarashi, R. Y.; Laryukhin, M.; Doan, P. E.; Dos Santos, P. C.; Dean, D. R.; Seefeldt, L. C.; Hoffman, B. M. *J. Am. Chem. Soc.* **2004**, *126*, 9563.
(28) Lee, H.-I.; Sørlie, M.; Christiansen, J.; Yang, T.-C.; Shao, J.; Dean, D. R.; Hales, B. J.; Hoffman, B. M. *J. Am. Chem. Soc.* **2005**, *127*, 15880.
(29) Igarashi, R. Y.; Laryukhin, M.; Santos, P. C. D.; Lee, H.-I.; Dean, D. R.; Seefeldt, L. C.; Hoffman, B. M. *J. Am. Chem. Soc.* **2005**, *127*, 6231.
(30) Barney, B. M.; Laryukhin, M.; Igarashi, R. Y.; Lee, H.-I.; Santos, P. C. D.; Yang, T.-C.; Hoffman, B. M.; Dean, D. R.; Seefeldt, L. C. *Biochemistry* **2005**, *44*, 8030.
(31) Barney, B. M.; Yang, T.-C.; Igarashi, R. Y.; Santos, P. C. D.; Laryukhin, M.; Lee, H.-I.; Hoffman, B. M.; Dean, D. R.; Seefeldt, L. C. *J. Am. Chem. Soc.* **2005**, *127*, 14960.
(32) Barney, B. M.; Lukoyanov, D.; Yang, T.-C.; Dean, D. R.; Hoffman, B. M.; Seefeldt, L. C. *Proc. Natl. Acad. Sci. U.S.A.* **2006**, *103*, 17113.
(33) Barney, B. M.; McClead, J.; Lukoyanov, D.; Laryukhin, M.; Yang, T. C.; Hoffman, B. M.; Dean, D. R.; Seefeldt, L. C. *Biochemistry* **2007**, *46*, 6784.
(34) Lukoyanov, D.; Yang, Z.-Y.; Dean, D. R.; Seefeldt, L. C.; Hoffman, B. M. *J. Am. Chem. Soc.* **2010**, *132*, 2526.
(35) Lukoyanov, D.; Barney, B. M.; Dean, D. R.; Seefeldt, L. C.; Hoffman, B. M. *Proc. Natl. Acad. Sci. U.S.A.* **2007**, *104*, 1451.
(36) DeRose, V. J.; Liu, K. E.; Lippard, S. J.; Hoffman, B. M. *J. Am. Chem. Soc.* **1996**, *118*, 121.
(37) Willems, J.-P.; Lee, H.-I.; Burdi, D.; Doan, P. E.; Stubbe, J.; Hoffman, B. M. *J. Am. Chem. Soc.* **1997**, *119*, 9816.
(38) Igarashi, R. Y.; Dos Santos, P. C.; Niehaus, W. G.; Dance, I. G.; Dean, D. R.; Seefeldt, L. C. *J. Biol. Chem.* **2004**, *279*, 34770.
(39) Huynh, B. H.; Henzl, M. T.; Christner, M. T.; Zimmerman, R.; Orme-Johnson, W. H.; Münck, E. *Biochem. Biophys. Acta* **1980**, *623*, 124.
(40) Given the success of Mössbauer spectroscopy in characterizing the ^{57}Fe ions of M^N, and the fact that it can determine isomer shifts and quadrupole couplings as well as hyperfine couplings, it is worth noting why this technique has not been applied to intermediates. The first difficulty is the presence of ^{57}Fe in both P and FeMo-co clusters, which makes it a challenge to extract the contributions from only FeMo-co. Although this has been overcome in studies of WT resting-state MoFe protein through selective ^{57}Fe enrichment of FeMo-co, the procedures are not practicable for the α-70Val→Ile MoFe protein. The second is that the resting M^N state in an as-isolated MoFe protein is present in 100% occupancy, whereas E_4 is trapped in the presence of other states of FeMo-co—not only residual M^N but also other, EPR-silent, yet Mössbauer-active, forms.
(41) Doan, P. E. *J. Magn. Reson.* **2011**, *208*, 76.
(42) Kinney, R. A.; Hetterscheid, D. G. H.; Hanna, B. S.; Schrock, R. R.; Hoffman, B. M. *Inorg. Chem.* **2010**, *49*, 704.
(43) Mouesca, J. M.; Noodleman, L.; Case, D. A.; Lamotte, B. *Inorg. Chem.* **1995**, *34*, 4347.
(44) Lee, H.-I.; Hales, B. J.; Hoffman, B. M. *J. Am. Chem. Soc.* **1997**, *119*, 11395.
(45) Christie, P. D.; Lee, H.-I.; Cameron, L. M.; Hales, B. J.; Orme-Johnson, W. H.; Hoffman, B. M. *J. Am. Chem. Soc.* **1996**, *118*, 8707.

(46) McLean, P. A.; True, A. E.; Nelson, M. J.; Lee, H.-I.; Hoffman, B. M.; Orme-Johnson, W. H. *J. Inorg. Biochem.* **2003**, *93*, 18.
(47) Christiansen, J.; Goodwin, P. J.; Lanzilotta, W. N.; Seefeldt, L. C.; Dean, D. R. *Biochemistry* **1998**, *37*, 12611.
(48) Burgess, B. K.; Jacobs, D. B.; Stiefel, E. I. *Biochim. Biophys. Acta* **1980**, *614*, 196.
(49) Seefeldt, L. C.; Morgan, T. V.; Dean, D. R.; Mortenson, L. E. *J. Biol. Chem.* **1992**, *267*, 6680.
(50) Seefeldt, L. C.; Rasche, M. E.; Ensign, S. A. *Biochemistry* **1995**, *34*, 5382.
(51) Werst, M. M.; Davoust, C. E.; Hoffman, B. M. *J. Am. Chem. Soc.* **1991**, *113*, 1533.
(52) Hoffman, B. M.; DeRose, V. J.; Ong, J. L.; Davoust, C. E. *J. Magn. Reson.* **1994**, *110*, 52.
(53) Davoust, C. E.; Doan, P. E.; Hoffman, B. M. *J. Magn. Reson.* **1996**, *119*, 38.
(54) Brueggemann, W.; Niklas, J. R. *J. Magn. Reson., Ser.A* **1994**, *108*, 25.
(55) Schweiger, A.; Jeschke, G. *Principles of Pulse Electron Paramagnetic Resonance*; Oxford University Press: Oxford, UK, 2001.
(56) Epel, B.; Arieli, D.; Baute, D.; Goldfarb, D. *J. Magn. Reson. (San Diego, CA: 1997* **2003**, *164*, 78.
(57) Epel, B.; Gromov, I.; Stoll, S.; Schweiger, A.; Goldfarb, D. *Concepts Magn. Reson., Part B* **2005**, *26B*, 36.
(58) Silakov, A.; Reijerse, E. J.; Albracht, S. P. J.; Hatchikian, E. C.; Lubitz, W. *J. Am. Chem. Soc.* **2007**, *129*, 11447.
(59) Mehring, M.; Hoefer, P.; Grupp, A. *Ber. Bunsen-Ges. Phys. Chem.* **1987**, *91*, 1132.
(60) Goldfarb, D.; Epel, B.; Zimmermann, H.; Jeschke, G. *J. Magn. Reson.* **2004**, *168*, 75.
(61) When nuclear relaxation is rapid, difference Triple is instead used for determination of relative signs of hyperfine couplings.
(62) Möbius, K.; Lubitz, W.; Plato, M. In *Advanced EPR. Applications in Biology and Biochemistry*; Hoff, A. J., Ed.; Elsevier: Amsterdam - Oxford - New York - Tokyo, 1989; p 441.
(63) Bennebroek, M. T.; Schmidt, J. *J. Magn. Reson.* **1997**, *128*, 199.
(64) Epel, B.; Poppl, A.; Manikandan, P.; Vega, S.; Goldfarb, D. *J. Magn. Reson.* **2001**, *148*, 388.
(65) Yang, T.-C.; Hoffman, B. M. *J. Magn. Reson.* **2006**, *181*, 280.
(66) Doan, P. E. Manuscript in preparation.
(67) Lee, H.-I.; Cameron, L. M.; Hales, B. J.; Hoffman, B. M. *J. Am. Chem. Soc.* **1997**, *119*, 10121.
(68) Lee, H.-I.; Sorlie, M.; Christiansen, J.; Song, R.; Dean, D. R.; Hales, B. J.; Hoffman, B. M. *J. Am. Chem. Soc.* **2000**, *122*, 5582.
(69) Venters, R. A.; Nelson, M. J.; McLean, P. A.; True, A. E.; Levy, M. A.; Hoffman, B. M.; Orme-Johnson, W. H. *J. Am. Chem. Soc.* **1986**, *108*, 3487.
(70) Mouesca, J. M.; Noodleman, L.; Case, D. A. *Inorg. Chem.* **1994**, *33*, 4819.
(71) We are aware that for some FeS systems, the values of $|a_{test}|$ are larger. For example, for aconitase and various heterometallic clusters ($[MFe_3S_4]^{n+}$, M = V, Mo, Co, Ni), generally $|a_{test}| > 30$ MHz (ref 43).
(72) In either case, the hyperfine couplings of a proton bound to sulfide are expected to be small, and the ENDOR signals from such protons would be indistinguishable from those of the exchangeable protons associated with nearby amino acid residues.
(73) Lowe, D. J.; Fisher, K.; Thorneley, R. N. F. *Biochem. J.* **1990**, *272*, 621.
(74) Lukoyanov, D.; Dikanov, S. A.; Yang, Z.-Y.; Barney, B. M.; Samoilova, R. I.; Narasimhulu, K. V.; Dean, D. R.; Seefeldt, L. C.; Hoffman, B. M. *J. Am. Chem. Soc.* **2011**, *133*, 11655.
(75) We acknowledge an anonymous reviewer for calling this proposal, "bold".
(76) Beinert, H.; Holm, R. H.; Munck, E. *Science* **1997**, *277*, 653.
(77) Kennedy, M. C.; Stout, C. D. *Adv. Inorg. Chem.* **1992**, *38*, 323.
(78) Dance, I. *Inorg. Chem.* **2011**, *50*, 178.
(79) Lee, H.-I.; Cameron, L. M.; Christiansen, J.; Christie, P. D.; Pollock, R. C.; Song, R.; Sorlie, M.; Orme-Johnson, W. H.; Dean, D. R.; Hales, B. J.; Hoffman, B. M. *ACS Symp. Ser.* **2003**, *858*, 150.